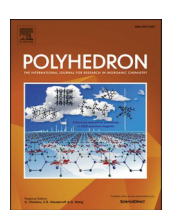


Contents lists available at ScienceDirect

# Polyhedron

journal homepage: www.elsevier.com/locate/poly





# Steric congestion in heavy pnictines alters oxidative halogenation pathways

John S. Wenger, Addis Getahun, Timothy C. Johnstone

Department of Chemistry and Biochemistry, University of California Santa Cruz, Santa Cruz, CA 95064, USA

#### ARTICLE INFO

Keywords: Main-group Antimony Bismuth Stiborane Bismuthorane

#### ABSTRACT

Dihalotriorganopnictoranes serve as important synthetic precursors in Group 15 chemistry, but the influence of the organic substituents on the synthesis and reactivity of these compounds remains underexplored for the heavy pnictogens. We recently reported the isolation of Dipp<sub>3</sub>Sb (Dipp = 2,6-diisopropylphenyl). The bulky Dipp substituents permit the isolation of monomeric tetrahedral stibine oxide Dipp<sub>3</sub>SbO, yet also allow for the formation of the trigonal bipyramidal Dipp<sub>3</sub>SbF<sub>2</sub>. We now report the isolation of a sterically crowded bismuthine, Dipp<sub>3</sub>Bi. Reaction between Dipp<sub>3</sub>Bi and XeF<sub>2</sub> afforded Dipp<sub>3</sub>BiF<sub>2</sub>, which features a distorted trigonal bipyramidal geometry in the solid state. Reaction between Dipp<sub>3</sub>Bi and PhICl<sub>2</sub> resulted in the generation of 1-chloro-2,6-diisopropylbenzene. Reaction between Dipp<sub>3</sub>Sb and PhICl<sub>2</sub> resulted in the formation of Dipp<sub>3</sub>SbCl<sub>2</sub>, which features a square pyramidal geometry in the solid state. Mes<sub>3</sub>SbCl<sub>2</sub>, Mes<sub>3</sub>SbBr<sub>2</sub>, Mes<sub>3</sub>BiBr<sub>2</sub> (Mes = mesityl) were structurally characterized and all exhibit trigonal bipyramidal geometries in the solid state. Solution-phase spectroscopic measurements reflect the fluxionality of all of these molecules, but theoretical analyses in the gas phase suggest that the square pyramidal geometry of Dipp<sub>3</sub>SbCl<sub>2</sub> is more thermodynamically favorable than the trigonal bipyramidal geometry, possibly due to the presence of intramolecular secondary interactions between the Dipp and Cl substituents. These results highlight the ability of Dipp substituents to alter reactivity pathways of heavy pnictines.

# 1. Introduction

Investigation of the Group 15 elements, the pnictogens, is in a state of rejuvenation following recent realizations of exciting reactivity that can be harnessed from carefully designed main-group compounds [1]. The variable coordination numbers and facile access to multiple oxidation states enjoyed by the pnictogens invite comparisons to transition-metal chemistry [2–6]. Of particular note are pnictogen compounds that can access variable redox states to effect catalytic chemical transformations, as well as compounds that exhibit extreme Lewis acidity that can be exploited for practical applications [7-14]. For example, catalytic hydrodefluorination of aryl C-F bonds has been achieved via an oxidative addition/reductive elimination pathway at a Cs-symmetric phosphorous triamide and an N,C,N-pincer complex of Bi(I) [15,16]. Although the catalytic redox chemistry of phosphorus is dominated by cycling between the +3 and +5 oxidation states, examples of Bi(I/III), Bi (II/III), and Bi(III/V) cycles have been reported in recent years [7.8.17.18].

Pnictogen chemistry also has a rich history in medicine. The clinically approved drug, brigatinib, features a dimethylphosphine oxide

moiety that imparts salutary pharmacokinetic properties relative to more traditionally used polar groups [19]. Arsenic trioxide is a clinically approved treatment for acute promyelocytic leukemia, and nanomaterial delivery platforms are in development to further expand its therapeutic potential [20]. The antimonial drugs meglumine antimoniate (Glucantime) and sodium stibogluconate (Pentostam) are used to treat the neglected tropical disease leishmaniasis; the molecular structures of these compounds are hitherto unknown but under intense investigation [21]. The role of bismuth in medicine is perhaps most widely known because of bismuth subsalicylate (Pepto-Bismol), a globally marketed gastrointestinal medication, but compounds of bismuth are also under investigation for the treatment of viral and bacterial infections [22]. Furthermore, efforts are being made toward the design of  $\mathrm{Bi}^{3+}$  chelators that can deliver  $\alpha$ -emitting  $^{213}\mathrm{Bi}$  nuclei to biological targets for cancer treatment [23,24].

Stibonium and bismuthonium species are of significant interest for their tunable Lewis acidity and have been explored for applications in ion sensing and catalysis [25–29]. An effective synthetic pathway towards  $\sigma^4, \lambda^5$  pnictonium species involves oxidative halogenation of a  $\sigma^3, \lambda^3$  triarylpnictine to form the  $\sigma^5, \lambda^5$  pnictorane, followed by a

E-mail address: johnstone@ucsc.edu (T.C. Johnstone).

 $<sup>^{\</sup>ast}$  Corresponding author.

metathesis reaction in which one pnictogen-bound halide is replaced by a weakly coordinating anion. In the resulting  $\sigma^4$ ,  $\lambda^5$  [Ar<sub>3</sub>PnX]<sup>+</sup> species, a low-lying Pn–X  $\sigma^*$  orbital is accessible from an open coordination site of the pnictogen cation [25]. An important feature for the design of these molecules is the choice of aryl substituent. If it does not provide enough steric protection, the species may undergo polymerization or other undesirable reactivity. If the aryl substituent is too large, then access to the  $\sigma^*$  orbital may be inhibited, attenuating substrate activation [30]. Either of the aforementioned situations may be desirable or undesirable and the pnictonium molecule must be carefully tuned to achieve the intended reactivity. A recent study employed careful ligand design to isolate a series of mono-, di-, and trinuclear fluorobismuthonium cations [28]. The authors reported that oxidative fluorination of trimesitylbismuthine (Mes<sub>3</sub>Bi) followed by halide abstraction resulted in the formation of a mononuclear fluorobismuthonium cation. In another study, a diverse series of triarylbismuthine species were treated with iodosobenzene (PhIO) [31]. Surprisingly, treatment of Mes<sub>3</sub>Bi with PhIO in dichloromethane (DCM) afforded the dichlorobismuthorane, Mes<sub>3</sub>BiCl<sub>2</sub>. In other cases, treatment of triarylbismuthines with PhIO afforded tetraarylbismuthonium salts, and in no cases did the authors isolate the expected bismuthine oxide. These results collectively highlight the importance of ligand design, as well as the curious reactivity of Bi(V)

Bulky aryl groups have been exploited with great success in the kinetic stabilization of highly reactive chemical motifs [32]. Heavy pnictogen atoms bearing bulky aryl substituents have served as important precursors in an array of fundamental and applied studies and, as noted above, oxidative halogenation is a staple reaction in pnictogen chemistry to access key intermediates in the synthesis of many interesting chemical motifs [21,25,33-37]. We recently prepared a very sterically encumbered stibine, Dipp<sub>3</sub>Sb (Dipp = 2,6-diisopropylphenyl), and demonstrated that the bulky Dipp substituents resulted in notable differences in reactivity relative to the less-encumbered Mes<sub>3</sub>Sb (Mes = mesityl) [38–40]. Oxidation of Dipp<sub>3</sub>Sb with PhIO afforded Dipp<sub>3</sub>SbO, the first example of an unperturbed monomeric stibine oxide [38]. The isolation of Dipp<sub>3</sub>SbO allowed for experimental verification of trends in pnictoryl (Pn<sup>+</sup>-O<sup>-</sup>) bonding, and Dipp<sub>3</sub>SbO was demonstrated to show a 10<sup>6</sup>-fold increase in Brønsted basicity over that of Dipp<sub>3</sub>AsO [41,42]. We were curious about how the oxidative halogenation of Bi(III) would change as a function of substituent bulk and how this change would compare to that in the corresponding antimony compounds.

Herein, we report the synthesis and characterization of the sterically encumbered bismuthine Dipp3Bi and describe its reactivity with the oxidative halogenation reagents XeF2 and iodobenzene dichloride (PhICl2). Treatment of Dipp3Bi with XeF2 resulted in the formation of the difluorobismuthorane Dipp3BiF2, whereas treatment of Dipp3Bi with PhICl<sub>2</sub> resulted in the formation of 1-chloro-2,6-diisopropylbenzene and other decomposition products. We then compared the reactivity of Dipp<sub>3</sub>Bi with that of a less sterically encumbered bismuthine, Mes<sub>3</sub>Bi, as well as the antimony-containing analogues Dipp<sub>3</sub>Sb and Mes<sub>3</sub>Sb. Treatment of Dipp<sub>3</sub>Sb with PhICl<sub>2</sub> resulted in the formation of Dipp<sub>3</sub>SbCl<sub>2</sub>, which exhibits a square pyramidal geometry in the solid state. Thermochemical calculations in the gas phase suggest that the square pyramidal geometry of Dipp<sub>3</sub>SbCl<sub>2</sub> is more thermodynamically stable than the trigonal bipyramidal geometry. Our results collectively highlight the interesting modulation of the reactivity of heavy pnictines by the steric congestion imposed by Dipp substituents.

# 2. Materials and methods

## 2.1. General methods

Reagents and solvents were purchased from commercial vendors and used as received unless otherwise specified. Mes<sub>3</sub>Sb, Mes<sub>3</sub>Bi, and Dipp<sub>3</sub>Sb were synthesized following literature protocols [28,38,43]. DCM and tetrahydrofuran (THF) were purified using an Innovative

Technology PURE-SOLV solvent purification system. All solvents were dried over 3-Å molecular sieves. NMR spectra were collected using a Bruker Avance III HD 500 spectrometer equipped with a multinuclear Smart Probe. Signals in the <sup>1</sup>H and <sup>13</sup>C NMR spectra are reported in ppm as chemical shifts from tetramethylsilane and were referenced using the CHCl<sub>3</sub> (<sup>1</sup>H, 7.26 ppm) and CDCl<sub>3</sub> (<sup>13</sup>C, 77.16 ppm) solvent signals. The frequencies of <sup>19</sup>F NMR signals are reported in ppm as chemical shifts from CFCl<sub>3</sub> (referenced to 4-fluoroaniline at -126.88 ppm). The 4-fluoroaniline reference was an 87 µM solution in CDCl<sub>3</sub>, collected at 298 K. Infrared (IR) spectra were collected on KBr pellets using a Thermo Nicolet Nexus 870 FT-IR spectrometer. Mass spectrometry measurements were collected using an LTQ-Orbitrap Velos Pro MS instrument. In addition to NMR analyses, the purity of novel materials was confirmed by observing agreement between experimental PXRD data of freshly prepared bulk solid and simulated powder diffraction patterns from single-crystal structures.

## 2.2. Synthesis of tris(2,6-diisopropylphenyl)bismuthine (Dipp<sub>3</sub>Bi)

A dry 250 mL two-necked round bottom flask fitted with a waterjacketed Liebig condenser was charged with a stir bar and magnesium turnings (771 mg, 31.7 mmol). Under an atmosphere of N2, the magnesium turnings were suspended in dry THF (40 mL) and activated with 1,2-dibromoethane (690 µL, 8.0 mmol). 1-Bromo-2,6-diisopropylbenzene (4.8 mL, 23 mmol) was added dropwise and the reaction was refluxed for 3 h. After the magnesium turnings had been consumed, the colorless solution was cooled to -78 °C and CuCl (2.36 g, 23.8 mmol) was added against a backflow of N2 with an additional 15 mL of THF. The reaction mixture was allowed to warm to room temperature and stir overnight to form a pale white suspension. The resulting suspension was cooled to -78 °C and a suspension of trichlorobismuthine (2.490 g, 7.900 mmol) in THF (10 mL) was then added dropwise to the reaction mixture. The reaction mixture was stirred at room temperature for 30 min before being refluxed for 19 h. The resulting dark green suspension was cooled to room temperature, opened to air, and diluted with OEt2 (150 mL) and water (200 mL). The aqueous layer was back-extracted with  $OEt_2$  (2  $\times$  50 mL). The combined organic phases were then washed with water (2  $\times$  200 mL) and with brine (250 mL). The organic layer was dried over Na2SO4. The solvent was removed under reduced pressure. The resulting yellow oil was diluted with hexanes, filtered through Celite, and purified by flash chromatography (SiO<sub>2</sub>, 1:20 ethyl acetate: hexanes). The collected fractions were stripped of solvent to obtain a yellow oil. Yellow crystals grew from the oil and were washed with acetonitrile and collected by vacuum filtration. Yield: 0.587 g (11%). Crystals suitable for X-ray diffraction were obtained similarly. M. p. 208 °C (decomp.). **ESI-MS** (m/z) [M-Dipp] + 531.246 (calc 531.246). <sup>1</sup>H NMR (500 MHz, CDCl<sub>3</sub>)  $\delta$  7.28 (br s, 9H), 3.14 (br s, 6H), 1.5–0.25 (br m, 36H).  $^{13}C\{^{1}H\}$  NMR (125 MHz, CDCl<sub>3</sub>)  $\delta$  162.68, 156.68, 155.17, 128.37, 125.25, 123.65, 41.86, 37.63, 26.76, 24.93, 24.48, 23.52. In addition to NMR data, purity was confirmed by PXRD data from freshly prepared bulk solid; these powder data agreed with the simulated powder diffractogram generated from the crystal structure of Dipp<sub>3</sub>Bi (Fig. S4).

# 2.3. Synthesis of difluorotris(2,6-diisopropylphenyl)bismuthorane (Dipp<sub>3</sub>BiF<sub>2</sub>)

A solution of  $XeF_2$  (13.1 mg, 0.0774 mmol) in DCM (0.6 mL) was added dropwise to a yellow solution of  $Dipp_3Bi$  (51.5 mg, 0.0743 mmol) in DCM (0.6 mL). Bubbling occurred and the yellow color subsided. After 5 min, hexamethyldisiloxane (5 mL) was added and the solvent level was reduced to induce crystallization. Colorless crystals grew overnight. The solvent was decanted and the crystals were washed with 1 mL hexamethyldisiloxane before being dried under vacuum. Yield: 27 mg (50%). Crystals suitable for X-ray diffraction were obtained similarly. M.p. 178 °C. **ESI-MS** (m/z) [M–F]  $^+$  711.377 (calc 711.377).  $^1$ H

NMR (500 MHz, CDCl<sub>3</sub>)  $\delta$  7.42 (s, 9H), 3.37 (br hept, J = 7.0 Hz, 6H), 1.26 (d, J = 5.9 Hz, 18H), 1.09 (d, J = 6.4 Hz, 18H). <sup>13</sup>C{<sup>1</sup>H} NMR (125 MHz, CDCl<sub>3</sub>)  $\delta$  167.38, 153.73, 130.72, 127.56, 36.06, 27.18, 24.51. <sup>19</sup>F{<sup>1</sup>H} NMR (470 MHz, CDCl<sub>3</sub>)  $\delta$  –65.85. In addition to NMR data, purity was confirmed by PXRD data from freshly prepared bulk solid; these powder data agreed with the simulated powder diffractogram generated from the crystal structure of Dipp<sub>3</sub>BiF<sub>2</sub> (Fig. S9).

# 2.4. Synthesis of dichlorotris(2,6-diisopropylphenyl)stiborane (Dipp<sub>3</sub>SbCl<sub>2</sub>)

A solution of Dipp<sub>3</sub>Sb (49 mg, 0.081 mmol) in DCM (0.6 mL) was added dropwise to a solution of PhICl2 (24 mg, 0.088 mmol) in DCM (0.6 mL). The yellow iodobenzene dichloride solution immediately became colorless and the solution was passed through Celite with an additional 1 mL of DCM for quantitative transfer. Pentane (10 mL) was added and the solvent was stripped to yield a colorless crystalline solid. The product was washed with pentane (2 x 1 mL) and dried under vacuum. Crystals suitable for X-ray diffraction were grown by slow evaporation of a mixture of DCM/pentane. Yield: 30 mg, 58%. M.p. 167 °C. **ESI-MS** (m/z)  $[M-Cl_2+OH]$  + 621.305 (calc 621.305) (HR-MS experiment only detected hydrolysis product Dipp<sub>3</sub>SbOH<sup>+</sup> highlighting the instability of this species). <sup>1</sup>H NMR (500 MHz, CDCl<sub>3</sub>)  $\delta$  7.38 (s, 3H), 7.28 (d, J = 5.7 Hz, 6H), 3.58 (br s, 6H), 1.24 (d, J = 5.6 Hz, 18H), 0.99 (d, J = 6.1 Hz, 18H). <sup>13</sup>C{<sup>1</sup>H} NMR (125 MHz, CDCl<sub>3</sub>)  $\delta$  152.06, 130.92, 126.62, 36.47, 26.68, 24.17. In addition to NMR data, purity was confirmed by PXRD data from freshly prepared bulk solid; these powder data agreed with the simulated powder diffractogram generated from the crystal structure of Dipp<sub>3</sub>SbCl<sub>2</sub> (Fig. S13).

## 2.5. Reaction between Dipp3Bi and iodobenzene dichloride (PhICl2)

Dipp $_3$ Bi (8.2 mg, 0.011 mmol) and PhICl $_2$  (3.4 mg, 0.012 mmol) were dissolved in CDCl $_3$  (0.6 mL) to form a yellow solution. A colorless solid precipitated rapidly. After 2 h,  $^1$ H and  $^{13}$ C{ $^1$ H} NMR analyses revealed the generation of 1-chloro-2,6-diisopropylbenzene [44], along with other unknown decomposition products (Figs. S14, S15).

# 2.6. Crystal growth of dichlorotrimesitylbismuthorane cyclohexane solvate $[Mes_3BiCl_2\cdot(C_6H_{12})]$

Mes<sub>3</sub>BiCl<sub>2</sub> was synthesized according to a modified literature protocol [45]. Briefly, Mes<sub>3</sub>Bi (55 mg, 0.079 mmol) and PhICl<sub>2</sub> (24 mg, 0.087 mmol) were dissolved in DCM (3 mL) to form a colorless solution. After 5 min, cyclohexane (20 mL) was added, and the reaction mixture was filtered through a Celite pad. The solvent level was reduced under reduced pressure to induce crystallization of pale-yellow crystals that were suitable for X-ray diffraction. NMR analysis of the crystals match literature reported values for Mes<sub>3</sub>BiCl<sub>2</sub> [46]. <sup>1</sup>H NMR (500 MHz, CDCl<sub>3</sub>)  $\delta$  7.15 (s, 6H), 2.73 (s, 18H), 2.32 (s, 9H). <sup>13</sup>C{<sup>1</sup>H} NMR (125 MHz, CDCl<sub>3</sub>)  $\delta$  168.17, 141.98, 141.08, 132.24, 25.61, 20.94.

# Crystal growth of dibromotrimesitylbismuthorane chloroform solvate [Mes<sub>3</sub>BiBr<sub>2</sub>·(CHCl<sub>3</sub>)]

Mes<sub>3</sub>BiBr<sub>2</sub> was synthesized according to a modified literature protocol [45]. Mes<sub>3</sub>Bi (50 mg, 0.088 mmol) was dissolved in CHCl<sub>3</sub> (0.6 mL) and added to liquid Br<sub>2</sub> (15 mg, 0.095 mmol), resulting in a yellow solution. Vapor diffusion of pentane into the reaction mixture resulted in the precipitation of yellow crystals suitable for X-ray diffraction. Mes<sub>3</sub>. BiBr<sub>2</sub> has been reported and described as thermally unstable when dried, preventing many characterization techniques. <sup>1</sup>H NMR (500 MHz, CDCl<sub>3</sub>)  $\delta$  7.13 (s, 6H), 2.75 (s, 18H), 2.33 (s, 9H).

#### 2.8. Crystal growth of dichlorotrimesitylstiborane (Mes<sub>3</sub>SbCl<sub>2</sub>)

A solution of Mes<sub>3</sub>Sb (198 mg, 0.413 mmol) in DCM (2 mL) was added dropwise to a yellow solution of PhICl<sub>2</sub> (114 mg, 0.414 mmol) in DCM (1 mL). The colorless reaction mixture was passed through a Celite pad. The solvent was stripped to form a colorless solid. Recrystallization from hot hexanes afforded crystals suitable for X-ray diffraction. NMR analysis of the crystals match literature reported values for Mes<sub>3</sub>SbCl<sub>2</sub> [43]. <sup>1</sup>H NMR (500 MHz, CDCl<sub>3</sub>)  $\delta$  7.00 (s, 6H), 2.66 (s, 18H), 2.31 (s, 9H). <sup>13</sup>C{<sup>1</sup>H} NMR (125 MHz, CDCl<sub>3</sub>)  $\delta$  145.50, 142.34, 140.87, 131.09, 25.51, 21.01.

#### 2.9. Crystal growth of dibromotrimesitylstiborane (Mes<sub>3</sub>SbBr<sub>2</sub>)

A solution of Mes<sub>3</sub>Sb (192 mg, 0.400 mmol) in DCM (2 mL) was added dropwise to a solution of Br<sub>2</sub> (64.1 mg, 0.406 mmol) in DCM (1 mL). The yellow reaction mixture was stirred for 5 min before hexanes were added resulting in white precipitate that was collected via vacuum filtration. Recrystallization from hot hexanes afforded crystals suitable for X-ray diffraction. NMR analysis of the crystals match literature reported values for Mes<sub>3</sub>SbBr<sub>2</sub> [43]. <sup>1</sup>H NMR (500 MHz, CDCl<sub>3</sub>)  $\delta$  6.98 (s, 6H), 2.70 (s, 18H), 2.32 (s, 9H). <sup>13</sup>C{<sup>1</sup>H} NMR (125 MHz, CDCl<sub>3</sub>)  $\delta$  145.65, 142.12, 140.87, 131.16, 26.20, 20.97.

### 2.10. X-ray crystallography

Crystals of Dipp $_3$ Bi, Dipp $_3$ BiF $_2$ , Mes $_3$ BiCl $_2\cdot C_6H_{12}$ , Mes $_3$ BiBr $_2\cdot CHCl_3$ , Mes $_3$ SbCl $_2$ , Mes $_3$ SbBr $_2$ , and Dipp $_3$ SbCl $_2$  were grown as described above, selected under a microscope, loaded onto a MiTeGen polyimide sample loop using Paratone-N, and mounted onto a Rigaku XtaLAB Synergy-S single-crystal diffractometer. Each crystal was cooled to 100 K under a stream of nitrogen. Diffraction of Cu K $\alpha$  radiation from a PhotonJet-S microfocus source was detected using a HyPix6000HE hybrid photon counting detector. Screening, indexing, data collection, and data processing were performed with CrysAlisPro [47]. The structures were solved using SHELXT and refined using SHELXL following established strategies [48–50]. All non-H atoms were refined anisotropically. C-bound H atoms were placed at calculated positions and refined with a riding model and coupled isotropic displacement parameters (1.2 × U<sub>eq</sub> for non-methyl C—H atoms and 1.5 × U<sub>eq</sub> for methyl groups).

#### 2.11. Powder X-ray diffraction (PXRD)

Bulk samples of Dipp $_3$ Bi, Dipp $_3$ BiF $_2$ , and Dipp $_3$ SbCl $_2$  were ground using an agate mortar and pestle. The fine white powders were each loaded onto a MiTeGen polyimide sample loop using Paratone-N and mounted onto a Rigaku XtaLAB Synergy-S single-crystal diffractometer. The powder was cooled to 100 K under a stream of nitrogen. The diffraction of Cu K $\alpha$  radiation was collected while the sample underwent a Gandolfi scan. Data collection and processing were performed using CrysAlisPro. Simulated PXRD diffractograms were generated from the crystal structures of Dipp $_3$ Bi, Dipp $_3$ BiF $_2$ , and Dipp $_3$ SbCl $_2$  using Mercury and compared to the experimentally determined diffractograms.

# 2.12. Computational experiments

All geometry optimizations and frequency calculations were performed using ORCA 5.0.1 [51]. Geometry optimizations were performed on Dipp<sub>3</sub>BiF<sub>2</sub>, Dipp<sub>3</sub>SbF<sub>2</sub>, and Dipp<sub>3</sub>SbCl<sub>2</sub> starting from crystallographic coordinates employing the BP86 pure functional and def2-SVP basis set, with the RI approximation and def2/J auxiliary basis set [52]. The optimized coordinates were then used as a starting point for a subsequent geometry optimization using the PBE0 hybrid functional and def2-TZVPP basis set, with the RIJCOSX approximation and def2/J auxiliary basis set [53–57]. Frequency calculations were then performed at the same level of theory in the gas phase. We then optimized

Scheme 1. Synthesis of Dipp<sub>3</sub>Bi and oxidative fluorination to form Dipp<sub>3</sub>BiF<sub>2</sub>.

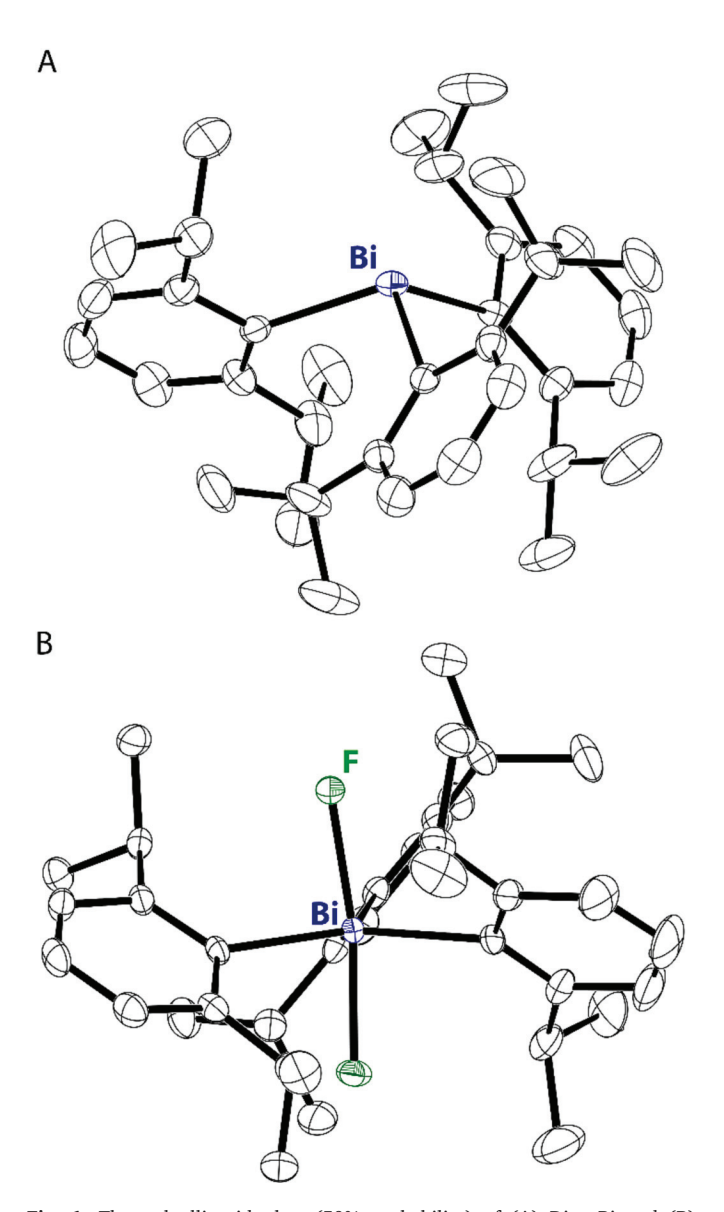


Fig. 1. Thermal ellipsoid plots (50% probability) of (A)  $Dipp_3Bi$  and (B)  $Dipp_3BiF_2$ . Color code: Bi navy, F light-green, and C black. Hydrogen atoms are omitted for clarity and only one of the crystallographically inequivalent molecules of  $Dipp_3BiF_2$  is depicted. ((Colour online.))

structures of Dipp<sub>3</sub>BiF<sub>2</sub>(linear) and Dipp<sub>3</sub>SbCl<sub>2</sub>(linear) starting from the coordinates of Dipp<sub>3</sub>SbF<sub>2</sub>, where the antimony or fluorine atoms were replaced by bismuth or chlorine, respectively, in order to find a minimum on the potential energy surface where the X–Pn–X bond angle approximates 180°. EDA was performed using Gaussian 09 [58]. Single point energy calculations (PBE0/QZVP) were performed on the 2Cl and Dipp<sub>3</sub>Sb fragments using coordinates from the optimized trigonal bipyramidal and square pyramidal structures.  $\Delta E_{tot}$  was obtained by subtracting the energies of the 2Cl and Dipp<sub>3</sub>Sb fragments from that of the Dipp<sub>3</sub>SbCl<sub>2</sub> molecule. MultiWFN (Version 3.7) was used to generate an input file for Dipp<sub>3</sub>SbCl<sub>2</sub> with an initial guess for the combined 2Cl

and Dipp $_3$ Sb fragments with no orbital interaction [59]. The energy of the initial guess wavefunction was subtracted from the final converged energy to obtain  $\Delta E_{\rm orb}$ . For the NCI analysis, single point energy calculations were performed using ORCA 5.0.1 on the optimized coordinates using the PBE0 hybrid functional and old-DKH-TZVPP allelectron, relativistically contracted basis set following the Douglass-Kroll-Hess formalism, with the RIJCOSX approximation and SARC/J auxiliary basis set [60–63]. Non-covalent interactions were calculated using MultiWFN and the results were visualized in VMD [64].

#### 3. Results and discussion

#### 3.1. Synthesis and fluorination of Dipp<sub>3</sub>Bi

We have previously synthesized Dipp<sub>3</sub>Pn (Pn = P, As, Sb) by adapting a protocol whereby 1-bromo-2,6-diisopropylbenzene is converted to an organocopper(I) reagent before the aryl group is installed on the pnictogen center (Scheme 1) [38,65]. Refluxing a mixture of BiCl<sub>3</sub> and the organocopper(I) reagent in THF resulted in the formation of a dark green suspension. Purification by liquid-liquid extraction and flash chromatography (SiO<sub>2</sub>/hexanes) yielded a yellow oil, from which yellow crystals of Dipp<sub>3</sub>Bi formed in 11% yield. The crystals were collected and washed with MeCN. <sup>1</sup>H and <sup>13</sup>C NMR spectroscopic analyses of the crystalline product revealed very broadened signals, consistent with a single Dipp environment and partially restricted rotation about the C<sub>ipso</sub>-Bi bond (Figs. S1, S2). The breadth of the resonances is also consistent with the reported <sup>1</sup>H NMR spectrum of Tipp<sub>3</sub>Bi (Tipp = 2,4,6-triisopropylphenyl) [65]. Interestingly, the NMR spectra of other Dipp<sub>3</sub>Pn (Pn = P, As, Sb) compounds show sharp, decoalesced signals indicating that rotation about the Cipso-Pn bond is slow on the NMR time scale. We suggest that the lengthening of the Pn-C<sub>ipso</sub> bond in the case of Bi reduces the energetic barrier of rotation, such that the signals have coalesced (<sup>1</sup>H) or broadened (<sup>13</sup>C) at room temperature. A single-crystal X-ray diffraction experiment (Fig. 1A) revealed that Dipp<sub>3</sub>Bi had crystallized in space group  $\overline{I4}3d$ . In the crystal, the molecules reside on crystallographic 3-fold rotation axes, allowing them to assume their full C<sub>3</sub> point-group symmetry. The crystallographically equivalent Bi-C bond lengths are 2.302(5) Å and the C-Bi-C bond angles are 106.16(12)°. The crystal structure of Dipp<sub>3</sub>Bi is isomorphous with the previously reported crystal structure of Dipp<sub>3</sub>Sb [38].

Difluorobismuthoranes have been well characterized and used as synthetic precursors, so we sought to similarly fluorinate  $Dipp_3Bi$  [28]. We previously reported the isolation of  $Dipp_3SbF_2$ , suggesting that the

**Table 1**Selected crystallographic metrics. [a]

Compound	X-Pn-X bond angle (°)	Pn–X bond length (Å)	τ parameter
Dipp <sub>3</sub> BiF <sub>2</sub>	169.68(6)/169.82(6)	2.1265(14)/2.1265	0.716(2)/0.723
		(14), 2.1132(14)/2.1099 (14)	(2)
Dipp <sub>3</sub> SbF <sub>2</sub> <sup>[b]</sup>	180.00(7)	1.971(3), 1.967(3)	1.00(2)
Dipp <sub>3</sub> SbCl <sub>2</sub>	154.89(2)	2.4864(4)	0.087(2)
Mes <sub>3</sub> BiF <sub>2</sub> <sup>[c]</sup>	179.00(4)	2.1222(10), 2.1223 (10)	0.954(1)
$Mes_3SbF_2^{[d]}$	179.53(5)	1.9821(10)	0.972(1)
Mes <sub>3</sub> BiCl <sub>2</sub>	180	2.645(6), 2.582(6)	1.00(2)
Mes <sub>3</sub> SbCl <sub>2</sub>	177.29(2)/178.55(3)	2.4976(7)/2.4810(8),	0.920(2)/0.929
		2.4790(7)/2.4748(8)	(2)
$Mes_3BiBr_2$	178.326(13)	2.8109(4), 2.7643(4)	0.913(3)
Mes <sub>3</sub> SbBr <sub>2</sub>	173.724(9)/177.953	2.6730(3)/2.6829(3),	0.839(2)/0.943
	(9)	2.6694(3)/2.6427(3)	(2)

[a] Values for crystallographically independent molecules are separated by slashes. [b] Crystallographic data of  $Dipp_3SbF_2$  were obtained from a prior report [38]. [c] Crystallographic data of  $Mes_3BiF_2$  were obtained from a prior report [28]. [d] Crystallographic data of  $Mes_3SbF_2$  were obtained from a prior report [25].

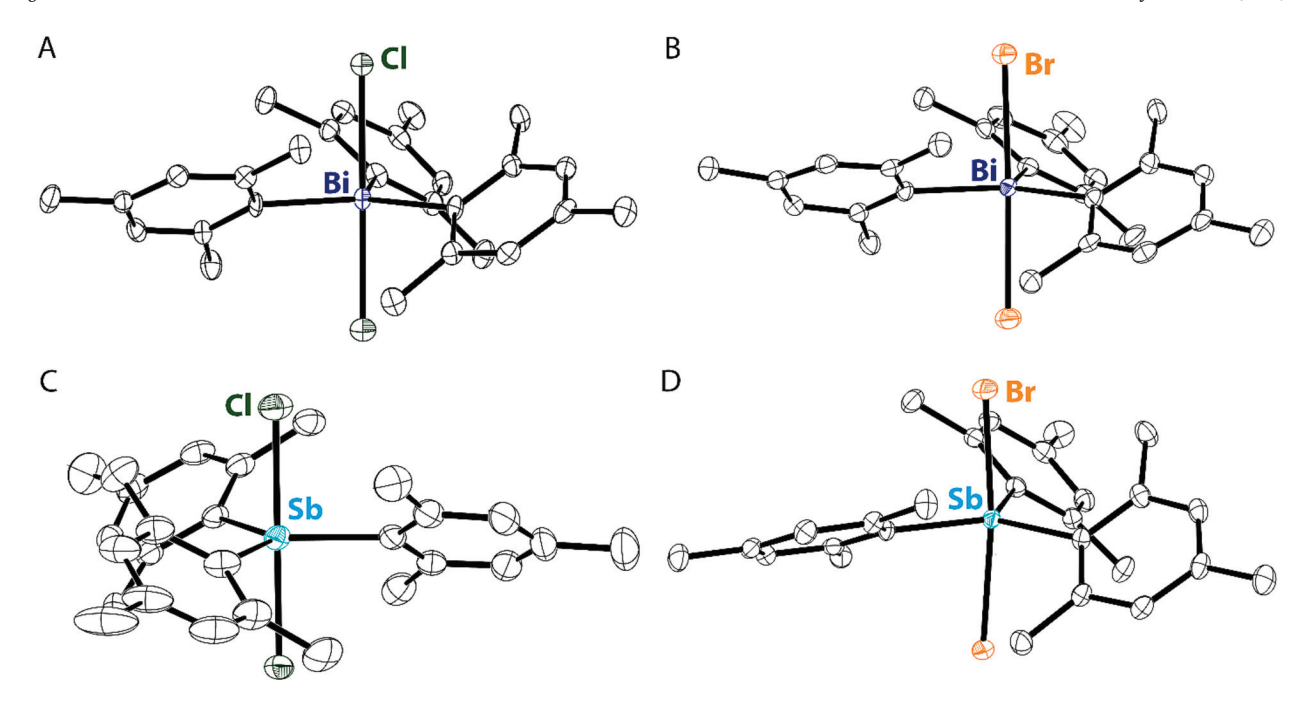


Fig. 2. Thermal ellipsoid plots (50% probability) of (A) Mes<sub>3</sub>BiCl<sub>2</sub>, (B) Mes<sub>3</sub>BiBr<sub>2</sub>, (C) Mes<sub>3</sub>SbCl<sub>2</sub>, and (D) Mes<sub>3</sub>SbBr<sub>2</sub>. Color code: Bi navy, Sb teal, Cl dark-green, Br orange, and C black. Hydrogen atoms are omitted for clarity. For C and D, only one of the crystallographically independent molecules is depicted. ((Colour online.))

steric environment imposed by the Dipp groups would not preclude the formation of the difluorobismuthorane [38]. Dropwise addition of a yellow DCM solution of Dipp<sub>3</sub>Bi to a DCM solution of  $XeF_2$  resulted in immediate effervescence and discharge of color from the solution. Addition of hexamethyldisiloxane to the reaction mixture followed by slow evaporation of the DCM afforded colorless crystals of Dipp<sub>3</sub>BiF<sub>2</sub> in a 50% yield.  $^1H$  and  $^{13}C$  NMR spectroscopic analyses of the product were consistent with the D<sub>3</sub> symmetry expected for a *trans*-dihalotriar-ylpnictorane (Figs. S5, S6).  $^{19}F$  NMR spectroscopy revealed a single signal at  $^{-65.85}$  ppm, significantly upfield of the fluorine resonances of both Mes<sub>3</sub>BiF<sub>2</sub> ( $^{-100.41}$  ppm) and Dipp<sub>3</sub>SbF<sub>2</sub> ( $^{-74.35}$  ppm) [28].

Dipp $_3$ BiF $_2$  crystallized in space group  $P\overline{1}$  with Z'=2 (Fig. 1B). Interestingly, the crystal structure of Dipp $_3$ BiF $_2$  features a bent F–Bi–F bond angle of 169.68(6)°/169.82(6)° (values are provided for both of the crystallographically independent molecules in the asymmetric unit), whereas Ph $_3$ BiF $_2$  and Mes $_3$ BiF $_2$  crystallize with almost perfectly linear F–Bi–F bond angles [28]. The  $\tau$  parameter 0.716(2)/0.723(2) captures the distorted trigonal bipyramidal geometry of Dipp $_3$ BiF $_2$  (Table 1). The Bi–F bond lengths of Dipp $_3$ BiF $_2$  are 2.1265(14)/2.1265(14) and 2.1132 (14)/2.1099(14) Å. Mes $_3$ BiF $_2$  features similar Bi–F bond lengths but a markedly less distorted trigonal bipyramidal geometry with a  $\tau$  parameter of 0.954(1).

### 3.2. Crystallographic characterization of dihalotrimesitylpnictoranes

In addition to the Mes $_3$ BiF $_2$  described above, Mes $_3$ Bi has been previously reported to undergo oxidation to form Mes $_3$ BiCl $_2$  or Mes $_3$ BiBr $_2$ , but a lack of crystallographic data prevented us from gaining comparative insight into the structures of the dihalotriarylbismuthoranes. Modifying literature procedures, we reprepared Mes $_3$ BiBr $_2$  and determined their crystal structures using single-crystal X-ray diffraction methods (Fig. 2A, B) [45]. For comparison, we also structurally characterized Mes $_3$ SbCl $_2$  and Mes $_3$ SbBr $_2$  (Fig. 2C, D) [25,43].

Mes $_3$ BiCl $_2$  crystallized as a cyclohexane solvate from a mixture of DCM and cyclohexane in space group P31c on a 3-fold rotation axis, crystallographically imposing linearity on the Cl–Bi–Cl angle. The Bi–Cl bond lengths are 2.645(6) and 2.582(6) Å. Mes $_3$ BiBr $_2$  crystallized as the yellow chloroform solvate from a mixture of chloroform and pentane in

space group  $P2_1/n$ . In our experience,  $Mes_3BiBr_2$  decomposes readily when removed from solvent, as has been noted previously [45]. The Br–Bi–Br bond angle is close to linear at  $178.326(13)^\circ$  and the Bi–Br bond lengths are 2.8109(4) and 2.7643(4) Å.

The antimony compounds  $Mes_3SbCl_2$  and  $Mes_3SbBr_2$  were each crystallized from hot hexanes, and both formed crystals in space group  $P\overline{1}$  with two molecules in the asymmetric unit.  $Mes_3SbCl_2$  features an almost linear Cl–Sb–Cl bond angle of  $177.29(2)/178.55(3)^\circ$  and the Sb–Cl bond lengths are 2.4976(7)/2.4810(8) and 2.4790(7)/2.4748(8) Å. Although the difference is subtle,  $Mes_3SbBr_2$  features a more bent X–Sb–X bond angle of  $173.724(9)/177.953(9)^\circ$  with Sb–Br bond lengths of 2.6730(3)/2.6829(3) and 2.6694(3)/2.6427(3) Å. We propose that the bromide substituents are sufficiently large to cause a significant steric repulsion with the Mes groups, such that the Br–Sb–Br bond angle distorts further from linearity. The structures of  $Mes_3SbCl_2$  and  $Mes_3SbBr_2$  are depicted in space-filling diagrams to highlight the difference in the size and steric environment of the halogen atoms (Fig. S24).

# 3.3. Oxidative chlorination of $Dipp_3Bi$ and $Dipp_3Sb$

With the structural data from the dihalotrimesitylstiboranes and dihalotrimesitylbismuthoranes in hand, we next attempted to oxidatively chlorinate Dipp<sub>3</sub>Bi with PhICl<sub>2</sub> (Scheme 1). Dissolution of Dipp<sub>3</sub>Bi and PhICl<sub>2</sub> in CDCl<sub>3</sub> under dry, air-free conditions resulted in the formation of a yellow solution. A colorless amorphous solid rapidly precipitated from the reaction mixture. We propose that the precipitate is composed of polymeric Bi-containing species [30,31].  $^{1}\mathrm{H}$  and  $^{13}\mathrm{C}$  NMR spectra of the supernatant reveal the generation of 1-chloro-2,6-diisopropylbenzene (Figs. S14, S15), which we suggest forms through a reductive elimination mechanism. We tentatively suggest that DippCl is generated by reductive elimination from a transient Bi(V) species, but we acknowledge that it could also arise from ligand exchange between Dipp<sub>3</sub>Bi and PhICl<sub>2</sub> and subsequent reductive elimination from the resulting I(III) species. We note the presence of other unidentified decomposition products in the supernatant (Figs. S14, S15). Bi(V) complexes frequently reduce to Bi(III) because of the stability of the latter, and electronegative substituents are often needed to stabilize Bi(V) compounds. The isolation of Mes<sub>3</sub>BiCl<sub>2</sub>

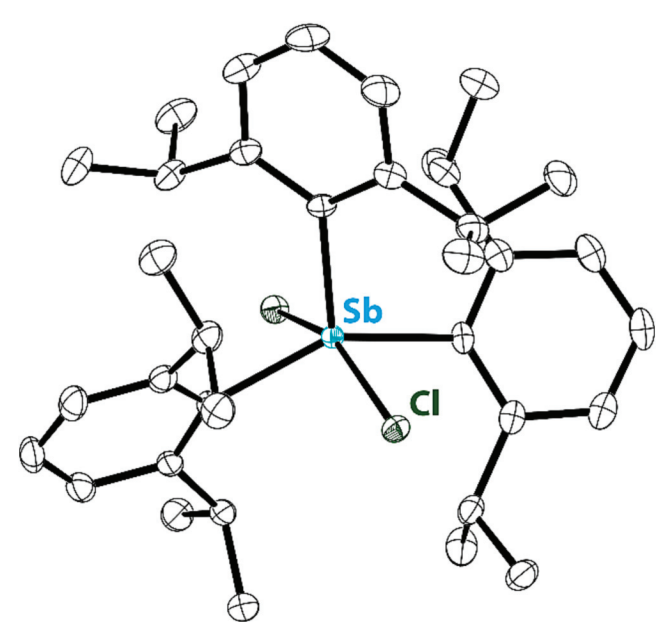
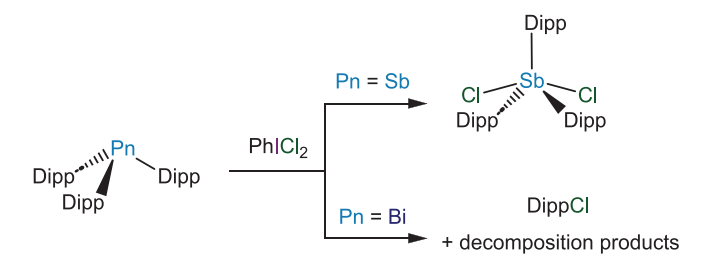


**Fig. 3.** Thermal ellipsoid plot (50% probability) of Dipp<sub>3</sub>SbCl<sub>2</sub>. Color code: Sb teal, Cl dark-green, and C black. Hydrogen atoms are omitted for clarity. ((Colour online.))



Scheme 2. Oxidative chlorination of  $Dipp_3Sb$  and  $Dipp_3Bi$  with  $PhICl_2$ .

indicates that axial chloride substituents are sufficiently electronegative to stabilize a dichlorotriarylbismuthorane. Our findings suggest that it is the increased steric pressure imposed by the Dipp substituents that destabilizes the 5-coordinate Dipp3BiCl2 in favor of decomposition through a reductive elimination process. Other examples of reductive elimination from Bi(V) species have been reported [8]. The formation of the organic reductive elimination product indicates that the oxidation did indeed occur. It is possible that low-temperature experiments could permit the isolation of the bismuthorane but we have not yet had success in this regard. Because Sb(V) species are less prone to reductive elimination than Bi (V) species [7], we investigated the oxidation of Dipp<sub>3</sub>Sb with PhICl<sub>2</sub>. Addition of a colorless DCM solution of Dipp<sub>3</sub>Sb to a yellow DCM solution of PhICl<sub>2</sub> resulted in the immediate loss of color. Addition of pentane to the reaction mixture, followed by slow evaporation of the DCM resulted in the formation of colorless crystals of Dipp<sub>3</sub>SbCl<sub>2</sub> in 50% yield. The <sup>1</sup>H and <sup>13</sup>C NMR spectra of the product are consistent with other symmetric dihalotriarylstiboranes, and an X-ray diffraction experiment unambiguously confirmed the identity of the species (Fig. 3, Scheme 2).

Dipp $_3$ SbCl $_2$  crystallizes in space group C2/c on a 2-fold rotation axis. Unlike Mes $_3$ SbCl $_2$ , which features a Cl–Sb–Cl bond angle of 177.29(2)°, Dipp $_3$ SbCl $_2$  features a Cl–Sb–Cl bond angle of 154.89(2)° in the solid-state. Dipp $_3$ SbCl $_2$  features a remarkably low  $\tau$  parameter of 0.087(2), indicating that this species can be appropriately characterized as square pyramidal. The crystallographic 2-fold rotation axis bisects the apical Dipp group. To the best of our knowledge, there are no other examples of dihalotriarylpnictoranes that have crystallized with a square pyramidal geometry. In all other cases, such as Dipp $_3$ SbF $_2$ , the apicophillic halide

ions reside in the axial positions of a trigonal bipyramid and the bulky aryl substituents occupy the equatorial positions. We suggest that the square pyramidal geometry of Dipp<sub>3</sub>SbCl<sub>2</sub>, as compared to e.g., Dipp<sub>3</sub>SbF<sub>2</sub>, arises from a combination of the extreme steric crowding of the Dipp groups, the larger size of the chloride ligands (as compared to fluoride), and the lower apicophillicity of chloride than fluoride. The decreased steric pressure exerted by mesityl substituents accounts for the trigonal bipyramidal structures of Mes<sub>3</sub>SbCl<sub>2</sub> and Mes<sub>3</sub>SbBr<sub>2</sub>.

# 3.4. Theoretical investigation of dihalopnictoranes

A natural question that arises during the analysis described above is whether the square pyramidal geometry assumed by Dipp $_3$ SbCl $_2$  in the crystal structure is simply a product of crystal packing forces. A gasphase geometry optimization (PBE0/def2-TZVPP) of Dipp $_3$ SbCl $_2$  starting from the crystallographic coordinates converged upon a square pyramidal geometry ( $\tau=0.10$ ), very similar to that in the crystal structure. This result confirms that the square pyramidal geometry is a local minimum on the potential energy surface (PES) of the compound, but not that it is the most stable geometry. A separate geometry optimization starting from a linear input structure confirmed that the linear structure (Cl–Sb–Cl angle of 179.62°) is also a local minimum on the PES. A thermochemical analysis indicated that square pyramidal was the more thermodynamically favored geometry; the square pyramidal geometry features a  $\Delta$ H that is 9.3 kcal/mol lower than that of the trigonal bipyramidal geometry (Table S3).

As described above, we had also noted that in the crystal structure of Dipp $_3$ BiF $_2$ , the crystallographically independent molecules exhibited slightly bent F–Bi–F angles of 169.68(6)° and 169.82(6)°. Geometry optimization starting from the crystallographic coordinates confirmed the distorted trigonal bipyramidal structure, albeit with an even more linear F–Bi–F bond angle of 173.04°. As with Dipp $_3$ SbCl $_2$ , we also optimized the structure of Dipp $_3$ BiF $_2$  starting from a linear input geometry, which converged upon a structure with a linear F–Bi–F angle of 180.00°. Thermochemical analysis of Dipp $_3$ BiF $_2$  determined the linear geometry to be slightly more thermodynamically stable, with a  $\Delta$ H that is 1.1 kcal/mol more stable than that of the distorted geometry (Table S3). The small difference in energies is consistent with the small difference in geometry, but nevertheless highlight the shallow nature of the PES.

To probe the underlying reasons for the enhanced thermodynamic stability of Dipp<sub>3</sub>SbCl<sub>2</sub> in the square pyramidal geometry relative to the trigonal bipyramidal geometry, we performed an energy decomposition analysis (EDA) of each geometry (PBE0/QZVP). The square pyramidal geometry could be stabilized by alleviation of steric repulsion or by the formation of more favorable bonding interactions relative to the trigonal bipyramidal state. We found that the ratio of  $\Delta E_{orb}/\Delta E_{total}$  was slightly greater in the square pyramidal geometry suggesting that the driving force could be the formation of more favorable bonding interactions, rather than attenuation of steric repulsion (Table S4).

We have previously shown that Dipp substituents engage in stabilizing intramolecular hydrogen bonding interactions in pnictine oxide and hydroxypnictonium species [38,41]. The EDA results above suggested that the geometries of Dipp<sub>3</sub>SbCl<sub>2</sub> and Dipp<sub>3</sub>BiF<sub>2</sub> that deviate from trigonal bipyramidal might also be stabilized by such intramolecular secondary interactions. We checked for their presence between the halides and the Dipp substituents using non-covalent interaction (NCI) analysis [66]. NCI analysis identifies regions of space between atoms where singularities in the reduced gradient of the electron density are present. The results of the analysis are typically depicted using isosurface plots. The isosurfaces are color-mapped with the function  $sign(\lambda_2)\rho$ , where  $\lambda_2$  is the second largest eigenvalue of the Hessian matrix, or Laplacian, and  $\rho$  is the electron density. Regions where sign  $(\lambda_2)\rho$  is close to 0 or negative represent attractive forces of strength comparable to hydrogen bonding interactions. Our NCI analysis of Dipp<sub>3</sub>SbCl<sub>2</sub> reveals the presence of attractive interactions between the

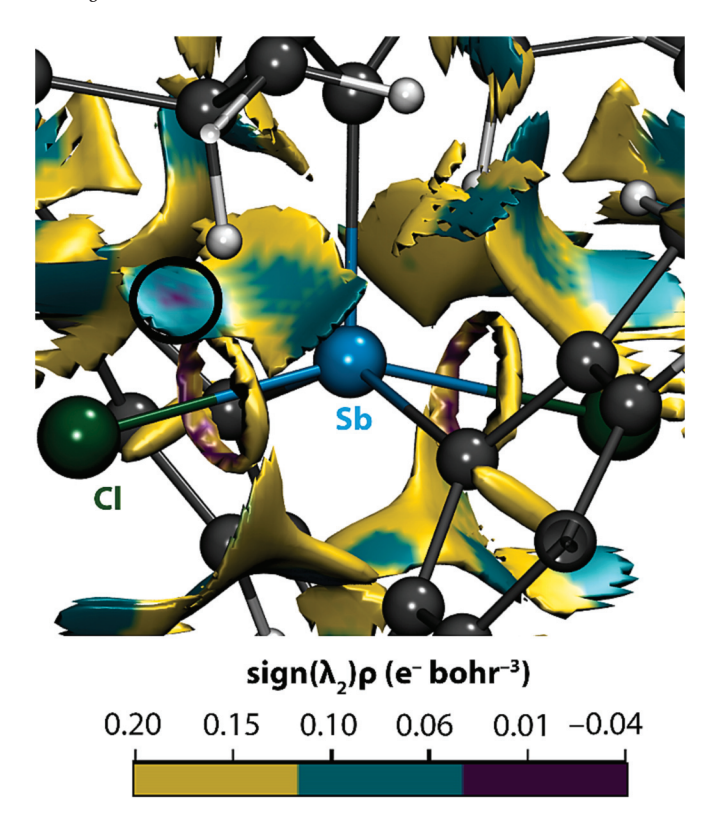


Fig. 4. NCI analysis of Dipp $_3SbCl_2$  depicting reduced gradient surfaces (isovalue = 0.45 a.u.) with the function  $sign(\lambda_2)\rho$  (where  $\lambda_2$  is the second-largest eigenvalue of the Laplacian) color-mapped on the surface. Purple is indicative of H-bonding interactions, aqua is indicative of van der Waals interactions, and yellow is indicative of steric repulsions. H-bonding interactions are highlighted with a black circle for clarity. Color code: Sb teal, Cl dark green, C black, H grey. ((Colour online.))

benzylic protons of the apical Dipp substituent and the chloride substituents (Fig. 4). We performed a similar analysis on Dipp $_3$ BiF $_2$  and found similar, albeit significantly weaker, attractive interactions between Dipp and fluoride substituents (Fig. S23). NCI analysis of Dipp $_3$ SbF $_2$  and the trigonal bipyramidal geometries of Dipp $_3$ SbCl $_2$  and Dipp $_3$ BiF $_2$  were also performed. In these cases, the NCI analysis indicates the presence of van der Waals interactions between the Dipp and halide substituents rather than stronger H-bonding interactions.

# 4. Conclusion

We have isolated and characterized a very sterically encumbered bismuthine, Dipp $_3$ Bi. Dipp $_3$ Bi was subject to oxidative halogenation reactions and was found to have reactivity remarkably different from that of Mes $_3$ Bi and Dipp $_3$ Sb. The reaction between Dipp $_3$ Bi and XeF $_2$  afforded a difluorobismuthorane with a bent F–Bi–F bond angle. The reaction between Dipp $_3$ Bi and PhICl $_2$  resulted in decomposition and the generation of products including 1-chloro-2,6-diisopropylbenzene. The reaction between Dipp $_3$ Sb and PhICl $_2$  resulted in the formation of Dipp $_3$ SbCl $_2$ , which features a highly unusual distorted square pyramidal geometry in the solid state. Theoretical data suggest that the square pyramidal geometry of Dipp $_3$ SbCl $_2$  is more thermodynamically stable than trigonal bipyramidal geometry. Ultimately, our results demonstrate the ability of bulky aryl substituents to modulate the reactivity of heavy pnictines.

# CRediT authorship contribution statement

**John S. Wenger:** Conceptualization, Methodology, Resources, Investigation, Validation, Writing – original draft, Writing – review &

editing, Visualization. Addis Getahun: Conceptualization, Methodology, Resources, Investigation, Validation, Writing – original draft, Writing – review & editing, Visualization. Timothy C. Johnstone: Conceptualization, Methodology, Resources, Investigation, Validation, Writing – original draft, Writing – review & editing, Visualization, Supervision, Project administration, Funding acquisition.

### **Declaration of Competing Interest**

The authors declare the following financial interests/personal relationships which may be considered as potential competing interests: Timothy C. Johnstone reports financial support was provided by National Science Foundation. Timothy C. Johnstone reports financial support was provided by American Chemical Society. Timothy C. Johnstone reports financial support was provided by Arnold and Mabel Beckman Foundation.

#### Data availability

Data will be made available on request.

#### Acknowledgements

The single-crystal X-ray diffractometer housed in the UCSC X-ray Diffraction Facility was funded by NSF MRI grant 2018501 and this work was further supported by the NSF through CAREER award 2236365, the ACS through PRF grant 66098-ND3, and Arnold and Mabel Beckman Foundation through a Beckman Young Investigator Award to T. C. J.

#### Appendix A. . Supplementary data

CCDC 2297429-2297430 contain the supplementary crystallographic data for  $Mes_3SbCl_2$ ,  $Mes_3SbBr_2$ ,  $Dipp_3Bi$ ,  $Mes_3BiBr_2 \cdot CHCl_3$ ,  $Dipp_3BiF_2$ ,  $Mes_3BiCl_2 \cdot C_6H_{12}$ , and  $Dipp_3SbCl_2$ . These data can be obtained free of charge via https://www.ccdc.cam.ac.uk/conts/retrieving. html, or from the Cambridge Crystallographic Data Centre, 12 Union Road, Cambridge CB2 1EZ, UK; fax: (+44) 1223-336-033; or e-mail: deposit@ccdc.cam.ac.uk.

# Appendix B. Supplementary data

Supplementary data to this article can be found online at https://doi.org/10.1016/j.poly.2023.116730.

#### References

- [1] P.P. Power, Main-group elements as transition metals, Nature 463 (2010) 171–177.
- [2] A.P.M. Robertson, S.S. Chitnis, H.A. Jenkins, R. McDonald, M.J. Ferguson, N. Burford, Establishing the Coordination Chemistry of Antimony(V) Cations: Systematic Assessment of Ph<sub>4</sub>Sb(OTf) and Ph<sub>3</sub>Sb(OTf)<sub>2</sub> as Lewis Acceptors, Chem.— Eur. J. 21 (2015) 7902–7913.
- [3] P.A. Gray, N. Burford, Coordination complexes of pnictogen(V) cations, Coord. Chem. Rev. 324 (2016) 1–16.
- [4] P.J. Sadler, H. Li, H. Sun, Coordination chemistry of metals in medicine: target sites for bismuth, Coord. Chem. Rev. 185–186 (1999) 689–709.
- [5] S.S. Chitnis, A.P.M. Robertson, N. Burford, B.O. Patrick, R. McDonald, M. J. Ferguson, Bipyridine complexes of  $E^{3+}$  (E = P, As, Sb, Bi): strong Lewis acids, sources of  $E(OTf)_3$  and synthons for  $E^I$  and  $E^V$  cations, Chem. Sci. 6 (2015) 6545–6555.
- [6] C. Lichtenberg, Molecular bismuth(III) monocations: structure, bonding, reactivity, and catalysis, Chem. Commun. 57 (2021) 4483–4495.
- [7] J.M. Lipshultz, G. Li, A.T. Radosevich, Main Group Redox Catalysis of Organopnictogens: Vertical Periodic Trends and Emerging Opportunities in Group 15, J. Am. Chem. Soc. 143 (2021) 1699–1721.
- [8] H.W. Moon, J. Cornella, Bismuth Redox Catalysis: An Emerging Main-Group Platform for Organic Synthesis, ACS Catal. 12 (2022) 1382–1393.
- [9] D. You, F.P. Gabbaï, Tunable σ-Accepting, Z-Type Ligands for Organometallic Catalysis, Trends Chem. 1 (2019) 485–496.
- [10] J.M. Bayne, D.W. Stephan, Phosphorus Lewis acids: emerging reactivity and applications in catalysis, Chem. Soc. Rev. 45 (2016) 765–774.

[11] L.T. Maltz, F.P. Gabbaï, Analyzing Fluoride Binding by Group 15 Lewis Acids: Pnictogen Bonding in the Pentavalent State, Inorg. Chem. 62 (2023) 13566–13572.

- [12] T.J. Hannah, W.M. McCarvell, T. Kirsch, J. Bedard, T. Hynes, J. Mayho, K. L. Bamford, C.W. Vos, C.M. Kozak, T. George, J.D. Masuda, S.S. Chitnis, Planar bismuth triamides: a tunable platform for main group Lewis acidity and polymerization catalysis, Chem. Sci. 14 (2023) 4549–4563.
- [13] S.S. Chitnis, F. Krischer, D.W. Stephan, Catalytic Hydrodefluorination of C–F Bonds by an Air-Stable P<sup>III</sup> Lewis Acid, Chem.–Eur. J. 24 (2018) 6543–6546.
- [14] L.S. Warring, J.E. Walley, D.A. Dickie, W. Tiznado, S. Pan, R.J. Gilliard, Lewis Superacidic Heavy Pnictaalkene Cations: Comparative Assessment of Carbodicarbene-Stibenium and Carbodicarbene-Bismuthenium Ions, Inorg. Chem. 61 (2022) 18640–18652.
- [15] S. Lim, A.T. Radosevich, Round-Trip Oxidative Addition, Ligand Metathesis, and Reductive Elimination in a P<sup>III</sup>/P<sup>V</sup> Synthetic Cycle, J. Am. Chem. Soc. 142 (2020) 16188–16193.
- [16] Y. Pang, M. Leutzsch, N. Nöthling, F. Katzenburg, J. Cornella, Catalytic Hydrodefluorination via Oxidative Addition, Ligand Metathesis, and Reductive Elimination at Bi(I)/Bi(III) Centers, J. Am. Chem. Soc. 143 (2021) 12487–12493.
- [17] M.B. Kindervater, K.M. Marczenko, U. Werner-Zwanziger, S.S. Chitnis, A Redox-Confused Bismuth(I/III) Triamide with a T-Shaped Planar Ground State, Angew. Chem. 131 (2019) 7932–7937.
- [18] A.D. Obi, D.A. Dickie, W. Tiznado, G. Frenking, S. Pan, R.J. Gilliard, A Multidimensional Approach to Carbodiphosphorane-Bismuth Coordination Chemistry: Cationization, Redox-Flexibility, and Stabilization of a Crystalline Bismuth Hydridoborate, Inorg. Chem. 61 (2022) 19452–19462.
- [19] W.-S. Huang, S. Liu, D. Zou, M. Thomas, Y. Wang, T. Zhou, J. Romero, A. Kohlmann, F. Li, J. Qi, L. Cai, T.A. Dwight, Y. Xu, R. Xu, R. Dodd, A. Toms, L. Parillon, X. Lu, R. Anjum, S. Zhang, F. Wang, J. Keats, S.D. Wardwell, Y. Ning, Q. Xu, L.E. Moran, Q.K. Mohemmad, H.G. Jang, T. Clackson, N.I. Narasimhan, V. M. Rivera, X. Zhu, D. Dalgarno, W.C. Shakespeare, Discovery of Brigatinib (AP26113), a Phosphine Oxide-Containing, Potent, Orally Active Inhibitor of Anaplastic Lymphoma Kinase, J. Med. Chem. 59 (2016) 4948–4964.
- [20] S.E. Hollow, T.C. Johnstone, Realgar and arsenene nanomaterials as arsenic-based anticancer agents, Curr. Opin. Chem. Biol. 72 (2023), 102229.
- [21] B. Lindquist-Kleissler, T.C. Johnstone, Models of the putative antimony(v)-diolate motifs in antileishmanial pentavalent antimonial drugs, Dalton Trans. 52 (2023) 9229–9237.
- [22] D.M. Griffith, H. Li, M.V. Werrett, P.C. Andrews, H. Sun, Medicinal chemistry and biomedical applications of bismuth-based compounds and nanoparticles, Chem. Soc. Rev. 50 (2021) 12037–12069.
- [23] D.J. Fiszbein, V. Brown, N.A. Thiele, J.J. Woods, L. Wharton, S.N. Macmillan, V. Radchenko, C.F. Ramogida, J.J. Wilson, Tuning the Kinetic Inertness of Bi<sup>3+</sup> Complexes: The Impact of Donor Atoms on Diaza-18-Crown-6 Ligands as Chelators for <sup>213</sup>Bi Targeted Alpha Therapy, Inorg. Chem. 60 (2021) 9199–9211.
- [24] J.J. Wilson, M. Ferrier, V. Radchenko, J.R. Maassen, J.W. Engle, E.R. Batista, R. L. Martin, F.M. Nortier, M.E. Fassbender, K.D. John, E.R. Birnbaum, Evaluation of nitrogen-rich macrocyclic ligands for the chelation of therapeutic bismuth radioisotopes, Nucl. Med. Biol. 42 (2015) 428–438.
- [25] M. Yang, F.P. Gabbaï, Synthesis and Properties of Triarylhalostibonium Cations, Inorg. Chem. 56 (2017) 8644–8650.
- [26] B. Pan, F.P. Gabbaï, [Sb(C<sub>6</sub>F<sub>5</sub>)<sub>4</sub>][B(C<sub>6</sub>F<sub>5</sub>)<sub>4</sub>]: An Air Stable, Lewis Acidic Stibonium Salt That Activates Strong Element-Fluorine Bonds, J. Am. Chem. Soc. 136 (2014) 9564–9567
- [27] M. Hirai, M. Myahkostupov, F.N. Castellano, F.P. Gabbaï, 1-Pyrenyl- and 3-Perylenyl-antimony(V) Derivatives for the Fluorescence Turn-On Sensing of Fluoride Ions in Water at Sub-ppm Concentrations, Organometallics 35 (2016) 1854–1860.
- [28] J. Kuziola, M. Magre, N. Nöthling, J. Cornella, Synthesis and Structure of Mono-Di-, and Trinuclear Fluorotriarylbismuthonium Cations, Organometallics 41 (2022) 1754–1762.
- [29] Y. Matano, S.A. Begum, T. Miyamatsu, H. Suzuki, A New and Efficient Method for the Preparation of Bismuthonium and Telluronium Salts Using Aryl- and Alkenylboronic Acids. First Observation of the Chirality at Bismuth in an Asymmetrical Bismuthonium Salt, Organometallics 17 (1998) 4332–4334.
- [30] S. Solyntjes, B. Neumann, H.-G. Stammler, N. Ignat'ev, B. Hoge, Difluorotriorganylphosphoranes for the Synthesis of Fluorophosphonium and Bismuthonium Salts, Eur. J. Inorg. Chem. 2016 (2016) 3999–4010.
- [31] H. Suzuki, T. Ikegami, N. Azuma, Unexpected formation of highly stabilized tetrakis-(2-alkoxyphenyl)bismuthonium salts in the oxidation of tris-(2alkoxyphenyl)bismuthanes with iodosylbenzene, J. Chem. Soc., Perkin Trans. 1 (1997) 1609–1616.
- [32] E. Rivard, P.P. Power, Multiple Bonding in Heavier Element Compounds Stabilized by Bulky Terphenyl Ligands, Inorg. Chem. 46 (2007) 10047–10064.
- [33] Y. Pang, N. Nöthling, M. Leutzsch, L. Kang, E. Bill, M. van Gastel, E. Reijerse, R. Goddard, L. Wagner, D. SantaLucia, S. DeBeer, F. Neese, J. Cornella, Synthesis and isolation of a triplet bismuthinidene with a quenched magnetic response, Science 380 (2023) 1043–1048.
- [34] M. Wu, W. Chen, D. Wang, Y. Chen, S. Ye, G. Tan, Triplet Bismuthinidenes Featuring Unprecedented Giant and Positive Zero Field Splittings, Natl. Sci. Rev. nwad169 (2023).
- [35] P. Šimon, F. De Proft, R. Jambor, A. Růzička, L. Dostál, Monomeric Organoantimony(I) and Organobismuth(I) Compounds Stabilized by an NCN Chelating Ligand: Syntheses and Structures, Angew. Chem., Int. Ed. 49 (2010) 5468-5471
- [36] P. Šimon, R. Jambor, A. Růžička, A. Lyčka, F. De Proft, L. Dostál, Monomeric organoantimony(III) sulphide and selenide with terminal Sb–E bond (E = S, Se).

- Synthesis, Structure and Theoretical Consideration, Dalton Trans. 41 (2012) 5140–5143.
- [37] O. Planas, F. Wang, M. Leutzsch, J. Cornella, Fluorination of arylboronic esters enabled by bismuth redox catalysis, Science 367 (2020) 313–317.
- [38] J.S. Wenger, M. Weng, G.N. George, T.C. Johnstone, Isolation, bonding, and reactivity of a monomeric stibine oxide, Nat. Chem. 15 (2023) 633–640.
- [39] J.S. Wenger, X. Wang, T.C. Johnstone, H-Atom Assignment and Sb–O Bonding of [Mes<sub>3</sub>SbOH][O<sub>3</sub>SPh] Confirmed by Neutron Diffraction, Multipole Modeling, and Hirshfeld Atom Refinement, Inorg. Chem. 60 (2021) 16048–16052.
- [40] J.S. Wenger, T.C. Johnstone, Unsupported monomeric stibine oxides (R<sub>3</sub>SbO) remain undiscovered, Chem. Commun. 57 (2021) 3484–3487.
- [41] J.S. Wenger, A. Getahun, T.C. Johnstone, Variation in pnictogen-oxygen bonding unlocks greatly enhanced Brønsted basicity for the monomeric stibine oxide, Dalton Trans. 52 (2023) 11325–11334.
- [42] B. Lindquist-Kleissler, J.S. Wenger, T.C. Johnstone, Analysis of Oxygen-Pnictogen Bonding with Full Bond Path Topological Analysis of the Electron Density, Inorg. Chem. 60 (2021) 1846–1856.
- [43] M. Ates, H.J. Breunig, A. Soltani-Neshan, M. Tegeler, Synthese von Mesitylstibanen / Synthesis of Mesitylstibanes, Z. Naturforsch., B. J. Chem. Sci., 41 (1986) 321-326.
- [44] T. Hoshi, T. Honma, A. Mori, M. Konishi, T. Sato, H. Hagiwara, T. Suzuki, An Active, General, and Long-Lived Palladium Catalyst for Cross-Couplings of Deactivated (Hetero)aryl Chlorides and Bromides with Arylboronic Acids, J. Org. Chem. 78 (2013) 11513–11524.
- [45] H. Gilman, H. Yablunky, Unsymmetrical Organobismuth Compounds, J. Am. Chem. Soc. 63 (1941) 207–211.
- [46] Y. Matano, H. Nomura, H. Suzuki, M. Shiro, H. Nakano, Synthesis, Structure, and Reactions of (Acylimino)triaryl-\(\lambda^5\)-bismuthanes: First Comparative Study of the (Acylimino)pnictorane Series, J. Am. Chem. Soc. 123 (2001) 10954–10965.
- [47] Rigaku Oxford Diffraction, CrysAlis<sup>Pro</sup>, (2020).
- [48] G.M. Sheldrick, SHELXT Integrated space-group and crystal-structure determination, Acta Crystallogr. Sect. A 71 (2015) 3–8.
- [49] G.M. Sheldrick, Crystal structure refinement with SHELXL, Acta Crystallogr. Sect. C 71 (2015) 3–8.
- [50] P. Müller, Practical suggestions for better crystal structures, Crystallogr. Rev. 15 (2009) 57–83.
- [51] F. Neese, The ORCA program package, Wiley Interdiscip, Rev.-Comput. Mol. Sci 2 (2012) 73–78.
- [52] A.D. Becke, Density-functional exchange-energy approximation with correct asymptotic behavior, Phys. Rev. A 38 (1988) 3098–3100.
- [53] J.P. Perdew, K. Burke, M. Ernzerhof, Generalized Gradient Approximation Made Simple, Phys. Rev. Lett. 77 (1996) 3865–3868.
- [54] J.P. Perdew, M. Ernzerhof, K. Burke, Rationale for mixing exact exchange with density functional approximations. J. Chem. Phys. 105 (1996) 9982–9985.
- [55] F. Weigend, R. Ahlrichs, Balanced basis sets of split valence, triple zeta valence and quadruple zeta valence quality for H to Rn: Design and assessment of accuracy, Phys. Chem. Chem. Phys. 7 (2005) 3297–3305.
- [56] F. Weigend, Accurate Coulomb-fitting basis sets for H to Rn, Phys. Chem. Chem. Phys. 8 (2006) 1057–1065.
- [57] F. Neese, F. Wennmohs, A. Hansen, U. Becker, Efficient, approximate and parallel Hartree-Fock and hybrid DFT calculations. A 'chain-of-spheres' algorithm for the Hartree-Fock exchange, Chem. Phys. 356 (2009) 98–109.
- [58] M.J. Frisch, G.W. Trucks, H.B. Schlegel, G.E. Scuseria, M.A. Robb, J.R. Cheeseman, G. Scalmani, V. Barone, G.A. Petersson, H. Nakatsuji, X. Li, M. Caricato, A.V. Marenich, J. Bloino, B.G. Janesko, R. Gomperts, B. Mennucci, H.P. Hratchian, J.V. Ortiz, A.F. Izmaylov, J.L. Sonnenberg, Williams, F. Ding, F. Lipparini, F. Egidi, J. Goings, B. Peng, A. Petrone, T. Henderson, D. Ranasinghe, V.G. Zakrzewski, J. Gao, N. Rega, G. Zheng, W. Liang, M. Hada, M. Ehara, K. Toyota, R. Fukuda, J. Hasegawa, M. Ishida, T. Nakajima, Y. Honda, O. Kitao, H. Nakai, T. Vreven, K. Throssell, J.A. Montgomery Jr., J.E. Peralta, F. Ogliaro, M.J. Bearpark, J.J. Heyd, E.N. Brothers, K.N. Kudin, V.N. Staroverov, T.A. Keith, R. Kobayashi, J. Normand, K. Raghavachari, A.P. Rendell, J.C. Burant, S.S. Iyengar, J. Tomasi, M. Cossi, J.M. Millam, M. Klene, C. Adamo, R. Cammi, J.W. Ochterski, R.L. Martin, K. Morokuma, O. Farkas, J.B. Foresman, D.J. Fox, Gaussian 16 Rev. D.01, in, Wallingford, CT, 2016.
- [59] T. Lu, F. Chen, Multiwfn: A multifunctional wavefunction analyzer, J. Comput. Chem. 33 (2012) 580–592.
- [60] D.A. Pantazis, X.-Y. Chen, C.R. Landis, F. Neese, All-Electron Scalar Relativistic Basis Sets for Third-Row Transition Metal Atoms, J. Chem. Theory Comput. 4 (2008) 908–919.
- [61] D.A. Pantazis, F. Neese, All-Electron Scalar Relativistic Basis Sets for the Lanthanides, J. Chem. Theory Comput. 5 (2009) 2229–2238.
- [62] D.A. Pantazis, F. Neese, All-Electron Scalar Relativistic Basis Sets for the Actinides, J. Chem. Theory Comput. 7 (2011) 677–684.
- [63] D.A. Pantazis, F. Neese, All-electron scalar relativistic basis sets for the 6p elements, Theor. Chem. Acc. 131 (2012) 1292.
- [64] W. Humphrey, A. Dalke, K. Schulten, VMD: Visual molecular dynamics, J. Mol. Graph. 14 (1996) 33–38.
- [65] S. Sasaki, K. Sutoh, F. Murakami, M. Yoshifuji, Synthesis, Structure, and Redox Properties of the Extremely Crowded Triarylpnictogens: Tris(2,4,6triisopropylphenyl)phosphine, Arsine, Stibine, and Bismuthine, J. Am. Chem. Soc. 124 (2002) 14830–14831.
- [66] E.R. Johnson, S. Keinan, P. Mori-Sánchez, J. Contreras-García, A.J. Cohen, W. Yang, Revealing Noncovalent Interactions, J. Am. Chem. Soc. 132 (2010) 6498–6506.